Geotechnical Testing Journal

doi:10.1520/GTJ20170251 / Vol. 41 / No. 3 / May 2018 / available online at www.astm.org

Zhijie Wang[1] and Radoslaw L. Michalowski[2]

An Apparatus for Testing Static Fatigue at Sand Grain Contacts

Reference

Wang, Z. and Michalowski, R. L., "An Apparatus for Testing Static Fatigue at Sand Grain Contacts," *Geotechnical Testing Journal*, Vol. 41, No. 3, 2018, pp. 448–458, https://doi.org/10.1520/GTJ20170251. ISSN 0149-6115

ABSTRACT

Often referred to as aging, the time-dependent evolution of silica sand properties is particularly distinct after sand disturbance. A likely cause of this behavior is the process of time-delayed fracturing of microscopic features at grain surfaces in contact. This process is denoted as static fatigue or stress corrosion microcracking. An apparatus was constructed to test time-dependent behavior of contacts subjected to sustained loads. The device can measure displacements with a resolution of about 100 nm. The focus of the paper is on the device constructed and not on the process of static fatigue. The details of apparatus construction are presented in the paper, and challenges associated with measuring grain deflection owing to static fatigue at the contacts are discussed. The measurements are sensitive to changes in temperature and humidity and are affected by external vibration excitations. Example results are illustrated, the sources of possible measurement errors are debated, and the challenges of testing are discussed.

Keywords

grain-scale testing, contact behavior, static fatigue, time dependence, silica sand

Manuscript received July 28, 2017; accepted for publication October 6, 2017; published online February 28, 2018.

[1] Country Garden Holdings Co. Ltd., Guangdong, China

[2] Department of Civil and Environmental Engineering, University of Michigan, 2028 G.G. Brown Bldg., Ann Arbor, MI 48109, USA (Corresponding author), e-mail: rlmich@umich.edu, https://orcid.org/0000-0002-9557-4802

Introduction

Time-dependent behavior of silica sand has been well documented, but the origin of this behavior is still not well understood. The presence of time effects in silica sand was indicated early in the measurements of shear wave velocity in sand subjected to sustained loads and in triaxial testing of specimens of sand subjected to isotropic consolidation for different periods prior to testing. The measurements of the speed of shear wave propagation in sand by Afifi and Woods (1971) (also Anderson and Stokoe [1978] and more recently Wichtmann and Triantafyllidis [2004]) clearly indicated a time-dependent increase of shear modulus in sand subjected to sustained load. A series of triaxial tests targeted at time effects in sand were carried out by Daramola (1980). Specimens of Ham River sand were loaded with a confining pressure of 400 kPa for 10, 30, and 152 days. The outcome of drained compression tests on these specimens indicated that, over time, the sand appeared to gain in stiffness but not as much in strength.

The early field observations of delayed response of a silica sand bed to a disturbance (compaction) were reported by Mitchell and Solymar (1984). The resistance of a silica sand bed to cone penetration

after dynamic compaction (vibro-compaction, explosives) did not increase immediately after disturbance, but it occurred over the weeks and months following the compaction process. The early hypothesis of mineral precipitation and bonding at contacts has not been confirmed, while the earlier search for the causes of the time effects in silica sand (Schmertmann 1991; Mesri, Feng, and Benak 1990) did not result in a proposal that would be generally agreed upon. Another piece of evidence for the time-dependent behavior of silica sand is related to setup of displacement piles (York et al. 1994; Chow et al. 1997; Bowman and Soga 2005; Jardine, Standing, and Chow 2006). The resistance of the pile shaft driven into silica sand can double within a year. Some attempts at explanation of this phenomenon included arching formation and subsequent relaxation of circumferential stress allowing time-dependent increase in radial stress on the pile shaft (Chow et al. 1997).

A hypothesis was suggested by Michalowski and Nadukuru (2012) that the phenomenon responsible for the time effects in silica sand is the delayed microfracturing of textural features (asperities and mineral fragments) on grain surfaces at contacts. This process has been referred to as static fatigue or stress corrosion cracking (Charles 1958; Scholz 1972; Wiederhorn and Bolz 1970; Michalowski and Nadukuru 2012; Wang and Michalowski 2015); it was also termed *contact maturing* (Michalowski, Wang, and Nadukuru 2018). The latter term was to disassociate the phenomenon from the negative connotation of *fatigue*, as the process leads to a beneficial outcome of increased stiffness. Static fatigue was considered by Lade and Karimpour (2010) as a cause of delayed fracturing of grains, contributing to time effects in silica sand.

In order to gain experimental evidence for the contact maturing hypothesis, an apparatus was constructed capable of measuring time-dependent behavior of grain contacts under sustained loads. A single sand grain is placed between two steel plates with parallel and relatively smooth surfaces, and the time-dependent increase in the deflection (also referred to as the *convergence* of the two surfaces) is measured while the two contacts are subjected to a stationary load. Under a load of no larger than several Newtons (well below grain crushing), the time-dependent convergence is attributed to the static fatigue process of silica occurring at the grain-loading platen contacts, with some contribution from the creep of the grain core material.

Grain-scale tests have been attempted by others (Cole and Peters 2008; Cole et al. 2010; Cavarretta, Coop, and O'Sullivan 2010; Cavarretta, Rocchi, and Coop 2011; Brzesowsky et al. 2011; Senetakis and Coop 2013; Wang and Coop 2016). However, past research was focused mainly on the immediate response of grains and contacts to load and crushability of grains. No attention has been paid to time-dependent properties and evolution of contacts under sustained loads, which is the key ingredient of the static fatigue hypothesis in Michalowski and Nadukuru (2012) and Wang and Michalowski (2015). Long-term experiments (weeks and months) present challenges associated with time-dependent behavior of mechanical components of the apparatus subjected to environmental loads. Quantitative measurements of the contact load-deflection behavior (indicative of contact response) are essential to understanding the contact properties and calibrating the contact constitutive models needed in simulations of grain assemblies.

Preliminary results from testing contacts of silica sand grains have already been published (Michalowski, Wang, and Nadukuru 2018), and this article is focused on the details of the custom-designed apparatus and its novelty and the challenges associated with the sensitivity of long-term measurements.

Apparatus

The original objective of constructing the apparatus was testing the time-dependent response of a single contact between two silica sand grains subjected to sustained (constant) load or the response of a contact of a silica grain with a hard and smooth surface. While the two contacts are not the same, they both are subjected to time-dependent response of the silica grain surface asperities, and thus both are indicative of the static fatigue (contact maturing) process. The early tests were performed in an apparatus constructed with four stages used to position the grains and to produce a single intergranular contact (Michalowski and Nadukuru 2014). However, the measurements in this apparatus were susceptible to inaccuracies caused by inherent tolerances in the moving components of the apparatus (stages) and creep of the adhesive that was necessary to attach the grains to the loading platens in the apparatus. Effectively, the apparatus measured the response of three contacts: one between the two grains and two contacts of the grains, each with one loading platen, with some involvement of the adhesive used to mount the grains. Consequently, a version of the apparatus was designed where no adhesive is used, and the number of moving parts is limited to a minimum. Rather than testing a contact between two grains, this newly constructed apparatus measures the simultaneous response of two contacts of one grain with two steel plates located on opposite sides of the grain (loading platens). The outcomes of such tests are indicative of the contact behavior, while eliminating some of the sources of inaccuracies and uncertainties in testing. The apparatus has only one high-quality stage (with one degree of freedom), and the stage is centrally loaded to avoid possibilities of rotation of its moving part. Also, the adhesive (glue) is no longer used to attach the grain to the steel surfaces in the device; rather, the grain rests between two horizontal steel surfaces without any adhesive. This apparatus is described in the next paragraphs.

A graphical rendering of the apparatus is shown in **Fig. 1a**. An L-shaped aluminum bracket [a] (depicted in **Fig. 1b**) with a vertical plate of height 152.4 mm is fastened to a 203.2- by 304.8- by 6.4-mm aluminum base plate [b] with four socket head screws.

FIG. 1 Schematic of testing apparatus: (a) general view and (b) components.

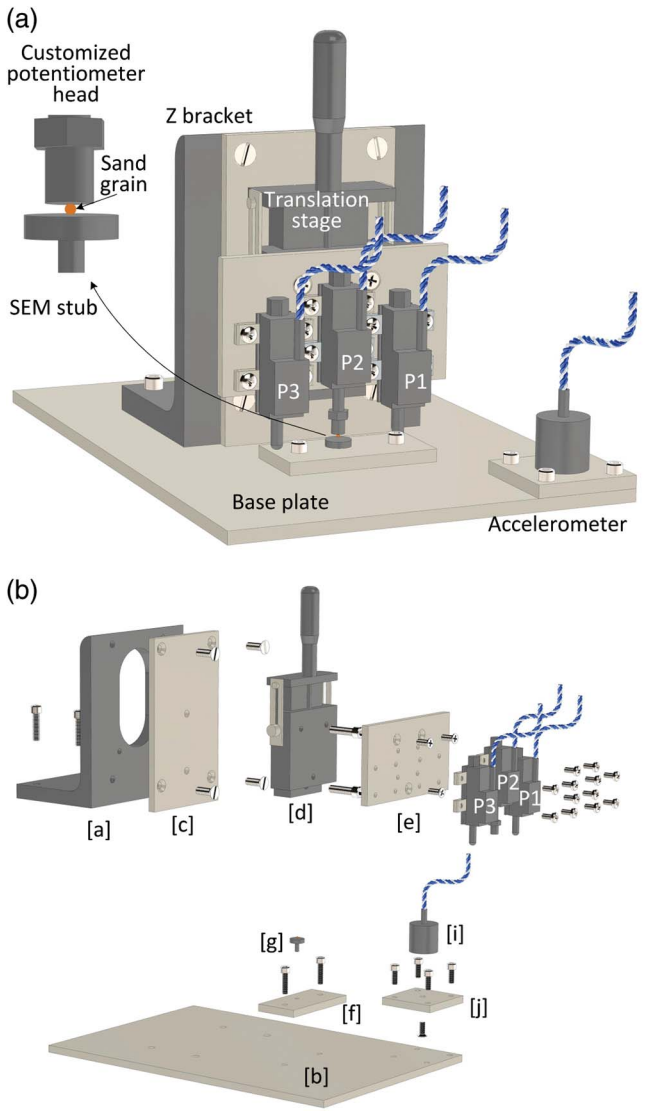

A 152.4- by 88.9- by 6.4-mm aluminum plate [c] is mounted on the vertical part of the bracket (with four flat countersunk head screws), and a stage [d] with manual micrometer control is fastened on the aluminum plate [c] (two socket head screws). This stage allows movement along the vertical axis. The stage provides a square flat mounting surface of 66.55 by 66.55 mm. An aluminum plate [e] (66.6 by 117.5 by 6.4 mm) is fastened on the stage (with three flat countersunk head screws) to provide enough surface area to mount three potentiometers. Potentiometers rather than linear variable differential transformers were used because of the authors' positive experience with potentiometers on the earlier generation of this apparatus. The potentiometers, labeled as P1, P2, and P3 (**Fig. 1**) are fastened to the aluminum plate [e], each using two clamps with four pan head screws. Under the potentiometers, a 76.2- by 38.1- by 6.4-mm aluminum plate [f] is fastened to the base plate [b] with two socket head screws. A stainless steel scanning electron microscope (SEM) specimen holding stub [g] with a threaded leg is mounted on plate [f] using a predrilled threaded opening.

The stage is driven by a metric micrometer with a traveling range of 25 mm. The potentiometers are contact-type position transducers with a 10-mm measuring range, and they track displacements using the position of the actuating shaft that is associated with the position of a slider on the resistor inside the potentiometer housing. The potentiometers are 17.5 mm in both height and width, and 76.0 mm in length.

The axis of symmetry of the SEM stub is aligned with that of the measuring arm of the central potentiometer P2. During tests, a sand grain is loaded between two horizontal stainless-steel surfaces: that of the SEM stub and that on the modified head of the arm of potentiometer P2 (see the upper-left corner insert in **Fig. 1a**). Potentiometer P2 performs two functions: (1) it exerts a required force on the grain, and for that purpose, the force-displacement characteristic of the spring in the potentiometer was calibrated and (2) it measures the change in the relative position of the two plates loading the grain (convergence). The two remaining potentiometers are used to detect whether any rotation of the stage has occurred, and they apply two symmetric forces to avoid any eccentricity in loading that might cause minute rotation of the moving part of the stage that is designed to have one degree of freedom (displacement in vertical direction).

An accelerometer [i] is mounted at one corner of the base plate to detect any vibrations that may cause undesired effects in the contact response. The accelerometer has a measurement range of ±5 *g* with a broadband resolution of 3 μ*g* root mean square (RMS). It has a sensitivity of 1,000 mV/*g* and its nonlinearity is less than 1 % (calculated as the maximum difference between the function value and its linear approximation). The excitation voltage is 18 to 30 V, constant current excitation is 2 to 10 mA, and the output impedance is less than 500 Ω. The accelerometer mass is 50 g and it is 24.6 mm in height and 25.1 mm in diameter. The accelerometer is first mounted on a 50.8- by 50.8- by 6.35-mm aluminum plate [j] with a flat countersunk head screw, and the plate with the accelerometer is fastened to the base plate with four socket head screws. This ensures its sensitivity to high-frequency vibrations. The base plate is placed on a 5-cm layer of porous polymeric damper to reduce transmission of external vibrations. A photograph of the device is presented in **Fig. 2**. This device was successfully used to test the time-dependent relative displacement of the two platens making contact with a grain while the grain was subjected to a constant load. The reduction in distance between the two plates loading the grain is referred to here as the *convergence*.

Potentiometer P2 was customized to meet the testing requirements; this involved two modifications. The first modification was replacing its default ball-point shaft head with a customized steel head with a flat surface. **Fig. 3** shows a disassembled

FIG. 2 A photograph of the assembled apparatus.

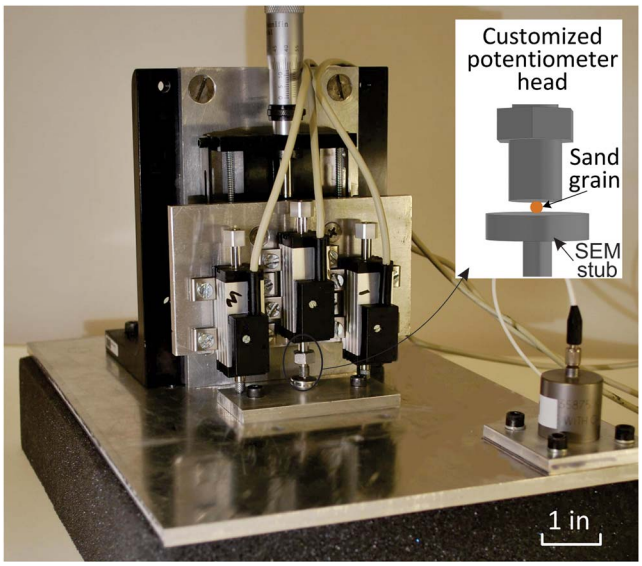

FIG. 3 Disassembled potentiometer.

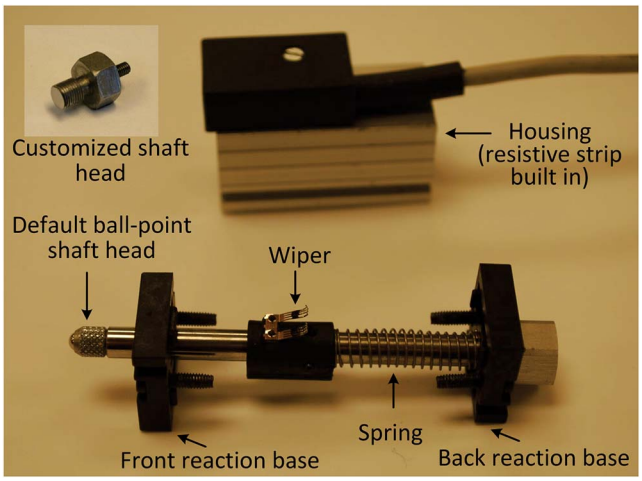

potentiometer, and the customized head is shown in the upper-left corner (see also upper-left corner insert in **Fig. 1a**). This modification was made to provide one of two platens loading the grain (the second platen being the SEM stub). The second modification included replacement of the standard spring in the potentiometer with one capable of generating desired forces within its working range without jeopardizing its position-measurement sensitivity (a standard spring used in this potentiometer typically requires a force larger than 2 N to activate the shaft). A linear and homogeneous relationship was found for the spring used (coefficient of determination R^2 of 0.9986)

$$F = 0.447\, d \tag{1}$$

where F is the force exerted by the measuring arm of potentiometer P2 (in N) and d is the displacement of the measuring rod from its zero position (in mm). The influence of convergence (typically, hundreds of nanometers) on the sustained force in the spring during testing was neglected.

Because of the sensitivity of static fatigue to temperature and humidity, the entire testing system is placed in an environmental chamber with temperature and humidity controlled during the testing period (typically weeks). To ensure consistent conditions during testing, temperature and relative humidity in the chamber are monitored with two independent temperature/humidity measurement sensors in addition to the sensors in the control system of the environmental chamber.

Data Acquisition System

The data acquisition system (DAQ) provides power sources and reads data from the potentiometers and the accelerometer. Each potentiometer is powered with a separate source with an input direct current (DC) voltage of 0.5 V, and the output voltage (0 to 0.5 V) is measured. The sampling rate of the output voltage measurements is 1 Hz. The displacement of the i-th potentiometer is converted from the voltage readings by the following:

$$d_{(i)} = D_{(i)} \cdot \left(V_{out(i)} / V_{in(i)}\right) \tag{2}$$

where $d_{(i)}$ is the displacement, $D_{(i)}$ is the measuring range, and $V_{out(i)}$ and $V_{in(i)}$ are the output and input voltages of the i-th potentiometer, respectively.

The DAQ system consists of four major modules accommodated in a chassis (all National Instruments components). The system has a 4-channel, 16-bit analog voltage output module A (voltage range ±10 V) powering the potentiometers; three independent 0.5-V DC voltages are provided by this module to the potentiometers. Modules B and C are two identical 4-channel 24-bit analog input modules to measure output voltages as well as input voltages of the potentiometers. Although module A provides nominal DC voltages of 0.5 V to the potentiometers, the actual output voltages of module A usually vary around the desired value with small drifts (using the power from a battery of an uninterrupted power supply did not help to reduce these fluctuations). Thus, both input and output voltages from each potentiometer are measured to calculate its displacement more accurately. Modules B and C take measurements from the potentiometers at a frequency of 1 Hz. The last module, D, is a 4-channel 24-bit current excitation and alternating current AC/DC input module. Module D is used for current excitation and taking measurements from the accelerometer with a 2.0 mA excitation current and a ±5-V AC/DC voltage measurement range. This module is connected to the coaxial connector of

the accelerometer through one of its 4 BNC connectors. The readings from the accelerometer are obtained at a frequency of 2 kHz.

The DAQ is controlled by a LabVIEW (National Instruments, Austin, TX) program installed on a portable PC, all placed in an environmental chamber. The computer is connected wirelessly to the Internet, and can be accessed remotely. The real-time readings of displacements and accelerations are shown on the LabVIEW interface and are monitored remotely to assure the tests are running without disturbances. With the wireless control of the portable computer, physical entries into the environmental chamber are avoided during tests, and this prevents a major source of external vibrations.

Testing Procedure

SAND GRAIN PREPARATION AND GRAIN LOADING

The sand grains are washed with a stream of distilled water to remove coarse debris from the surface, and then they are air-dried. Surface topography of the sand grains is characterized with SEM and atomic force microscopy (AFM) before each test. At least 24 h before being tested, a sand grain is placed in the environmental chamber to allow it to adapt to the temperature and the relative humidity in the testing chamber.

The sand grain to be tested is placed in the middle of the surface of the SEM stub (see upper-left insert in **Fig. 1a**), under the bottom surface of the rod head of potentiometer P2. Then the three potentiometers mounted on the stage are moved slowly downward using the manual stage micrometer until the flat rod tip surface of potentiometer P2 comes into contact with the grain that is resting below on a flat-surface SEM stub. Next, the grain becomes loaded with a required force. The target displacement of the stage, which generates the target force on the grain, is calculated from the calibration function, Eq 1. This target displacement is divided into four equal increments. During each increment, the stage is moved manually (using the stage micrometer) with a velocity averaging about 0.1 mm/s with a 1-min pause between increments. After the target displacement is reached, the stage is locked in position with two screws on both sides of the stage to maintain the force and to minimize undesired minute rotation of the stage in its rails allowed by the machining tolerances. This undesired motion is inherent even in stages that are designed to have only one degree of freedom; such motion can occur if the load on the potentiometer arm is not axial.

TEST DURATION AND CONVERGENCE MONITORING

During the test, the force is maintained at the desired level, with a negligible change caused by relaxation of the force in the spring due to grain deflection. Static fatigue caused by microfracturing in the contact asperities results in convergence of the two loading platens, thus some relaxation in the spring force of potentiometer P2. This effect on the normal force, however, is less than 1 mN (less than 0.1 % of a typical target force), as the fatigue-induced displacement is typically less than 2 μm. Ideally, a normal force would be maintained, but angularity of the grain and the surface texture at contacts may result in some departure from normality. However, the forces on the grain applied at the top and the bottom contacts must be collinear and equal in magnitude, as enforced by equilibrium. With the computer connected to a wireless network, the readings from the sensors are monitored remotely without anyone entering the chamber.

The test is stopped typically when the convergence of the two metallic surfaces hardly shows any change in three consecutive days. It was discovered from preliminary tests that this occurs after about 3 to 4 weeks. To make it easier to locate damage in the upper contact area after the test, a strong cyanoacrylate-based fast-acting adhesive is applied (through a needle) to the bottom contact to "freeze" the grain to the SEM stub. Then the grain is unloaded by unlocking and moving the translation stage upward in four reversed equal steps.

VISUALIZATION OF STATIC FATIGUE DAMAGE

An example of a contact region on a silica sand grain is illustrated in **Fig. 4a**; this grain was in contact with a glass plate, loaded with a force of 0.65 N for one week (Michalowski and Nadukuru 2012). This was a qualitative experiment, not in the apparatus described in this paper. The damage to a large asperity can be identified comparing the image before the loading in **Fig. 4b** to that after one week of sustained load in **Fig. 4c**. The post-test visual identification of static fatigue damage is challenging. In order to achieve this goal, zoomed-in SEM images of the contact area before and after the test are needed for comparison. However, the surface areas to be affected cannot be identified a priori, and the method requires scanning large portions of the grain surface with high resolution prior to the test. Monitoring evolution of the contact damage using AFM is not feasible, as it requires disassembling the contact for the purpose of scanning, with little chance of assembling it back to its original configuration. The challenge of monitoring damage progress may be overcome in the future with the use of high-resolution computed tomography scanning, but the authors did not find it achievable at this time.

Example Results

Although the focus of the paper is on the apparatus and not on the contact maturing process and test result, examples of data from the tests are presented in this section.

GRAINS USED IN TESTS

Ottawa 20-30 sand grains were used in contact fatigue tests. It is a silica sand with grain sizes between U.S. standard sieve sizes #20 and #30 (0.60 to 0.84 mm). A photograph of Ottawa 20-30 sand grains under an optical microscope is shown in **Fig. 5**. The

FIG. 4 (a) A contact region on a grain surface; (b) asperity before loading and (c) after loading with 0.65 N for one week (details of the test in Michalowski and Nadukuru 2012).

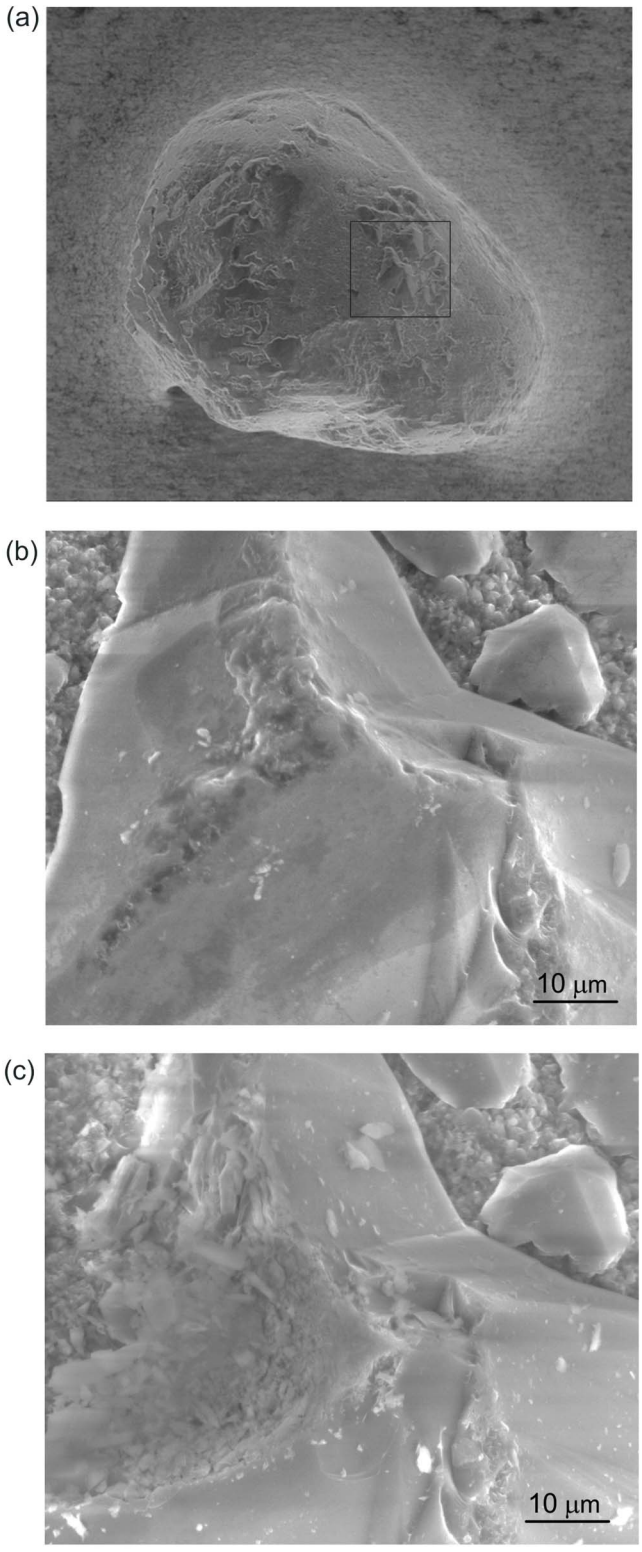

FIG. 5 Optical microscopic image of Ottawa 20-30 sand grains.

roundness of the grains was described by a Wadell's value of about 0.7 (Wadell 1932) by comparing the grains in **Fig. 5** to standard roundness charts (like those developed by Krumbein 1941).

The stainless-steel surfaces of the customized potentiometer head and the SEM stub were both polished using the same procedure to the same degree of smoothness. They were first sanded with 400 grit sandpaper to remove coarse asperities, then sanded further with 1,000 grit sandpaper and 2,500 grit sandpaper, and finally polished with a polishing paste and a polishing liquid. A mirror-type surface finish was achieved with this process.

The microscopic features of grain surfaces and stainless-steel surfaces were characterized with SEM and AFM. SEM images of the surface texture for a variety of sand grains of various origin can be found in Krinsley and Doornkamp (1973). **Fig. 6a** illustrates an AFM scan of a 30 by 30 μm region on an Ottawa sand grain. The roughness of the surface was characterized by the RMS of the surface elevation, defined as the following:

$$RMS = \sqrt{\frac{1}{mn}\sum_{i=1}^{m}\sum_{j=1}^{n}(z_{ij}-\mu)^2} \tag{3}$$

where μ is the average elevation of the surface:

$$\mu = \frac{1}{mn}\sum_{i=1}^{m}\sum_{j=1}^{n} z_{ij} \tag{4}$$

with m and n being the number of points in the scan in the x and y directions, respectively; z_{ij} is an elevation at the i-th column and

FIG. 6 AFM measurements: (a) scan of topography of a 30- by 30-μm region on Ottawa 20-30 sand grain, (b) scan of topography of the stainless-steel stub surface, and (c) cross-sectional profiles of the two surfaces.

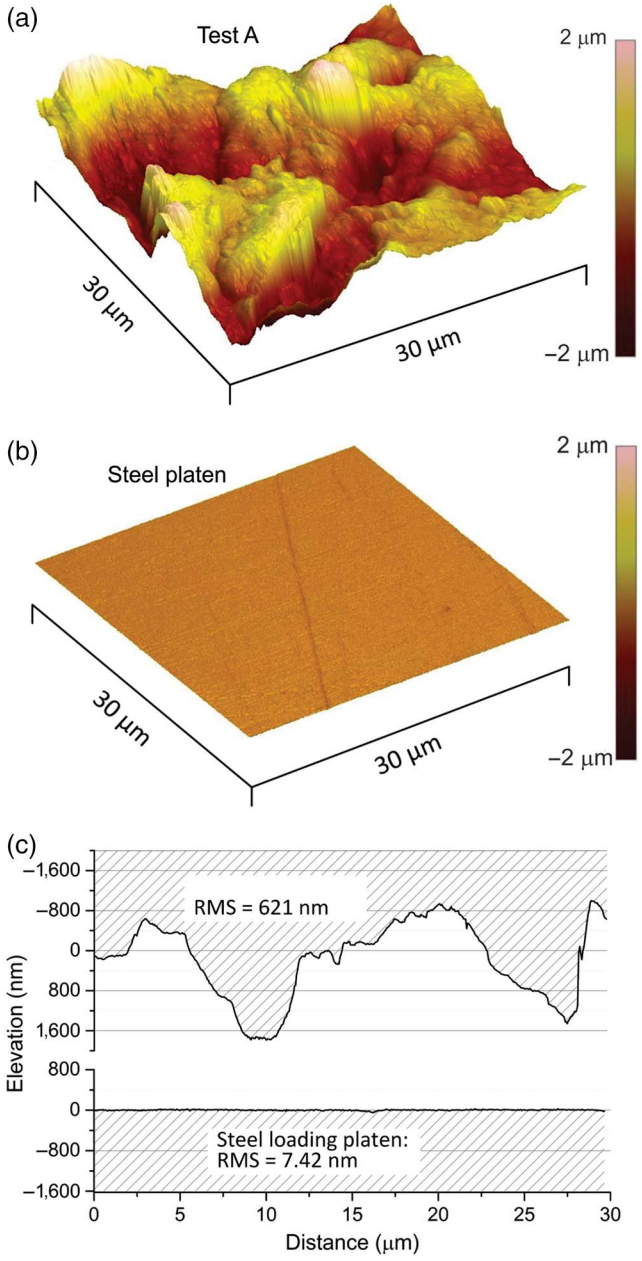

j-th row of the scan. This method was used to characterize initial roughness. When calculating RMS from the AFM scans, the average surface within the region of view (30 by 30 μm) was considered a flat surface. In addition to the grain surface topology in **Fig. 6a**, a scan of a loading platen is illustrated in **Fig. 6b**. Cross sections of the surface texture and the measurements of roughness for the two surfaces are shown in **Fig. 6c**.

FIG. 7 Time-dependent convergence results (data from Michalowski, Wang, and Nadukuru 2018); all Ottawa 20-30 sand grains loaded with 2.4 N: Test A—initial RMS = 621 nm, Test B—initial RMS = 321 nm, and Test C—initial RMS = 28.6 nm.

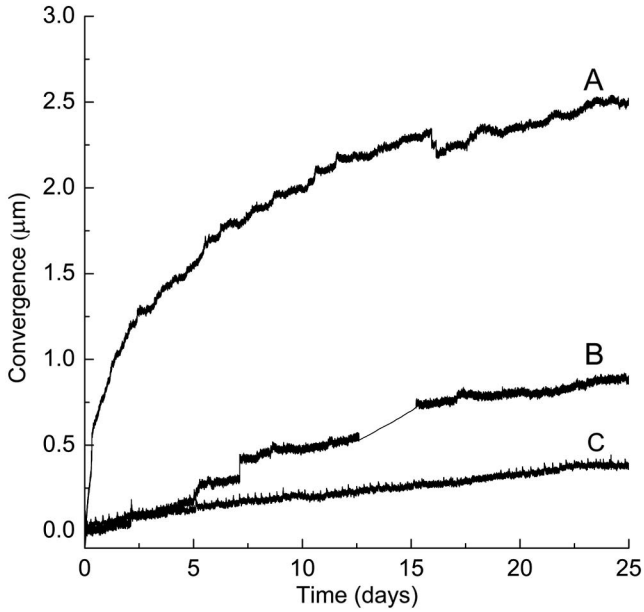

With an elevation RMS of 7.42 nm, the surface of the loading platen is two orders of magnitude smoother than the surface of the sand grain composed of random peaks and valleys, with an RMS of 621 nm.

RESULTS

The capability of the apparatus is shown in **Fig. 7** with examples of three tests; the convergence data for these tests are from Michalowski, Wang, and Nadukuru (2018). Plotted results are filtered using a moving average with a 5-point span (the noise was reduced from over 100 nm to about 50 nm). The tests marked A, B, and C were performed on grains with initial representative roughness measured by RMS equal to 621 nm, 321 nm, and 28.6 nm, respectively. The comparison of the tests indicates an important role of roughness in the process of static fatigue at the contacts. It is interesting to notice that the convergence of 2.38 μm in Test A after 20 days (**Fig. 7**) is close to the elevation amplitude in the grain surface profile in **Fig. 6c**, though it is too early to draw conclusions from this single observation (the reader will notice the convergence in **Fig. 7** is marked in μm, whereas the grain surface elevation in **Fig. 6c** is marked in nm). The tests were performed in a chamber with a controlled environment with a temperature of 20°C ± 1°C and relative humidity 30 ± 5 %. A loss of power was experienced between 12.5 and 15 days during Test B, but this did not change the trend of the curve. The convergence after 20 days

in tests A, B, and C reached 2.38 μm, 0.78 μm, and 0.31 μm, respectively. The average rate of convergence in the first day was about 15 nm/h in Test A, but this rate dropped to below 1 nm/h after about 3 weeks, as it did in the other two tests. This small rate of convergence is not dependent on the initial roughness of the grain, and it is likely to be associated with the creep of the core material of the grain. This paper is about the apparatus and testing intricacies, and not about the contact maturing itself. The reader will find a discussion of contact maturing and aging in silica sand elsewhere (Michalowski, Wang, and Nadukuru 2018).

Two abrupt changes in convergence were detected by potentiometer P2 in Test B: a small but distinct peak around day 2.2 and a sudden increase in convergence at day 7.1, as illustrated in **Fig. 7**. The accelerometer readings at these two instances were analyzed to identify any external vibrations that might be responsible for the sudden changes. These acceleration readings are shown in **Fig. 8**. The ambient acceleration (or the signal noise) is varying in the range of about ±0.02 *g*. The peak in convergence recorded at about 2.2 days from the start of the test does not appear to be associated with any vibrations caused by external sources, as indicated in **Fig. 8a**. This peak could have been caused by an electrical surge. However, three spikes up to ±0.06 *g* were recorded by the accelerometer during a 1.4-h time period around 7.1 days after the start of the test, **Fig. 8b**. This record will be analyzed at the end of the next section.

FIG. 8 Acceleration data from Test B: (a) 1.4-h time interval including an abrupt surge in convergence on day 2.2 and (b) 1.4-h time interval including an abrupt increase in convergence on day 7.1.

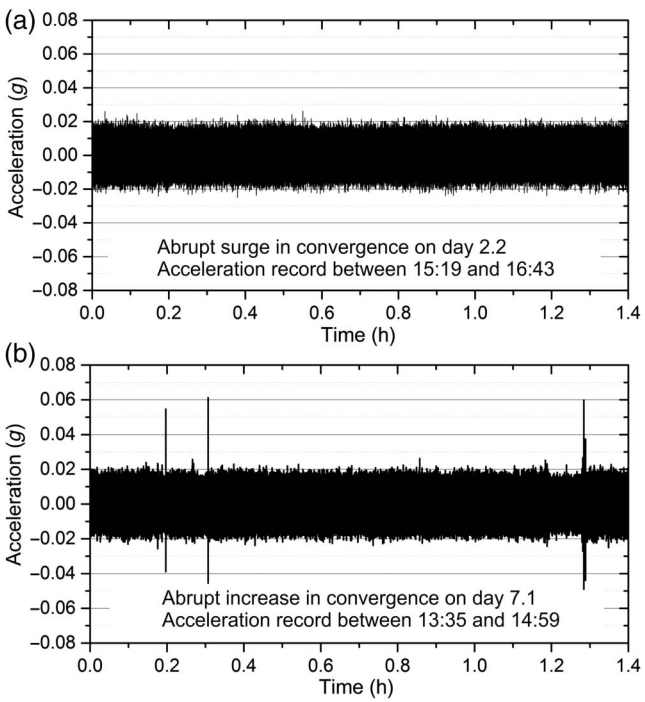

Inaccuracies in Measurements

Inaccuracies in measuring the outcome of the testing may come from external or internal sources. External factors are those due to changes in the environment, whereas internal factors refer to the performance of the mechanical and electrical components of the apparatus.

EXTERNAL FACTORS

These factors include changes in temperature and humidity, and also external vibrations. A 9-day test with a stainless-steel sphere was carried out in the constructed apparatus and subjected to varied temperature and relative humidity to investigate the sensitivity of the system to temperature and humidity. The sphere was 3.125 mm in diameter and was subjected to a constant force of 1.3 N. In earlier tests with a stainless-steel sphere under controlled temperature and relative humidity, no measurable convergence was detected (as expected); therefore, the measured effects in the test with varied temperature and humidity are attributed to the changes in the environment. The result of the test is shown in **Fig. 9**. As expected, no convergence was detected in the first day when the temperature and relative humidity were kept constant at 21°C and 36 %, respectively. In the second day, relative humidity was increased to 44 % while the temperature remained at 21°C. During this period, the reading of convergence increased steadily to reach 0.65 μm at the end of the second day. Stress corrosion cracking in silica is sensitive to changes in moisture content (Wiederhorn et al. 2014; Krauskopf 1959), but stainless steel is not expected to react in such a distinct fashion; the measured signal is likely to be the result of the effect of the change in humidity on the electrical system (Ciprian and Lehman 2009). In the subsequent 2 days, the relative humidity was set to 35 % with the temperature remaining at 21°C. During these two days, the

FIG. 9 Signal variation caused by a change in relative humidity and temperature in a test on a stainless-steel sphere (load: 1.3 N).

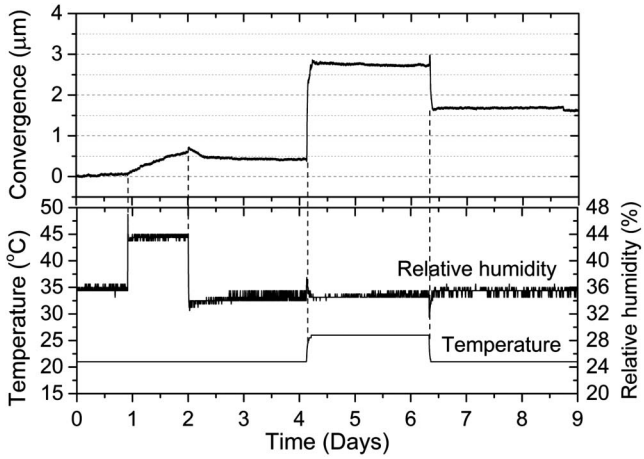

convergence reading recovered by 0.15 μm in the first 6 h and then remained at 0.5 μm. From the beginning of the 5th day through half of the 7th day, the temperature was set to 26°C without changing the relative humidity. The reading now shot up by 2.25 μm in about 2 h and had a steady value at 2.75 μm afterwards. As the temperature was set back to 21°C in the middle of day 7, convergence recovered by about 1.1 μm and remained at 1.65 μm in the remaining 2.5 days of the test. Although temperature and relative humidity both returned to their initial values, a nonzero reading of convergence was recorded at the end. It is evident that the variations in temperature and relative humidity cause changes in readings of potentiometer P2. This may be caused by expansion and contraction of the components of the apparatus (and the stainless-steel sphere), while the changes in humidity affect the electrical signal (Ciprian and Lehman 2009); the changes in humidity may, for instance, affect the electrical properties of the slider in the potentiometer. Simple calculations indicate that a 5°C change in temperature produces extension/contraction of the metal components of the apparatus that are greater than the magnitudes of expected convergence. Therefore, changes in temperature need to be avoided during testing. The influence of temperature on the long-term behavior of contacts (weeks) can be assessed from tests, each at a different but constant temperature. Changes in humidity and temperature do affect the rate of static fatigue in silica (Cuellar, Roberts, and Middleman 1987), but this effect might be difficult to distinguish from the effects caused by the inherent response of the apparatus and the electrical system to these changes.

As shown earlier in **Fig. 8b**, external vibrations are another environmental cause that may render interpretation of readings inaccurate. Such excitations can cause instant fracturing of the asperities at the contact, which will be manifested in sudden increases in convergence. The environmental sources of inaccuracies in measurements are mitigated by placing the entire apparatus in an environment chamber with controlled temperature and humidity (both constant) and by placing the device on a 5-cm thick foam-like damper to isolate the device, to some extent, from external vibrations.

INTERNAL FACTORS

Systematic inaccuracies in measurements caused by internal factors include two types: mechanical and electrical. Mechanical inaccuracies refer to undesirable, though minute movement of the device components. For instance, tolerances necessary for the stage to operate allow for minute relative rotation and transverse displacement in the rails of the moving component, even though the stage is designed to have only one degree of freedom in the vertical direction. To minimize this source of error in measurements, after the required force has been applied on the grain, the stage is locked in place symmetrically on two sides by two screws (standard stages typically come with a locking screw only on one side). The second type of systematic inaccuracies is a result of possible instability in electrical signal and signal drift. It is worthwhile to be aware of this source of errors, especially for static fatigue tests, which last several weeks. The potentiometers used in the apparatus were tested for long-term stability (weeks).

FIG. 10 Frequency content of acceleration measured during Test B during 1.4-h interval about day 7.1 (acceleration history shown in **Fig. 8b**).

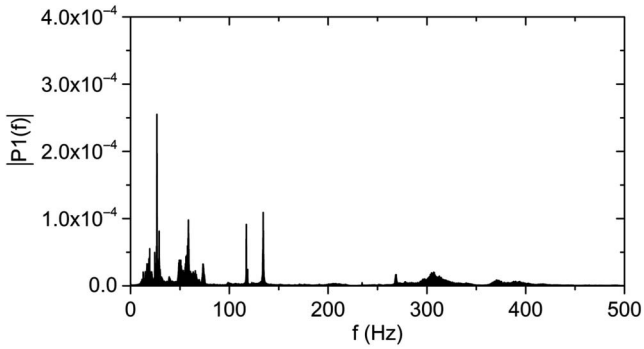

VIBRATION IDENTIFICATION

Fig. 10 shows the frequency (f) content of acceleration record illustrated in **Fig. 8b**. |P1(f)| represents the single-sided amplitude spectrum of the record in **Fig. 8b**, obtained from fast Fourier transformation (FFT). This is a 1.4-h excerpt from the record taken during the test marked as B in **Fig. 7**, about 7.1 days into the test, when a "jump" occurred in the measured convergence. In order to identify vibrations detected by the accelerometer during the test, a series of possible disturbance scenarios around the environmental chamber were simulated. A comparison of the acceleration readings from the tests to those from simulated vibrational events helps identify the sources of vibrations detected during tests. The vibrations simulated included opening and closing the chamber door, moving hardware, a person jumping off from a step of a certain height, walking or running heavily, knocking on or kicking the outside walls of the chamber, and dropping weights around the chamber. Acceleration data from two selected sources, both in time and frequency domains, are presented in **Fig. 11**. The acceleration data in the frequency domain were obtained from FFT of the acceleration data in the time domain. The results are from two events: opening and closing the door and running or walking heavily in the corridor adjacent to the environmental chamber. The background acceleration (or noise) is shown to be varying between −0.02 and 0.02 *g*, whereas the "event-generated" accelerations range from 0.045 to 0.09*g*, two to almost five times that of the accelerations of ambient vibrations.

To identify the sources of the vibration measured on day 7.1 in **Fig. 8b**, the frequency content of the reading (from FFT) was compared with those from simulated events. It appears that the frequency content of the event, **Fig. 10**, resembles that from opening and closing the door as shown in **Fig. 11c**. It is plausible that the

FIG. 11 Accelerometer readings and frequency content in simulated vibration events.

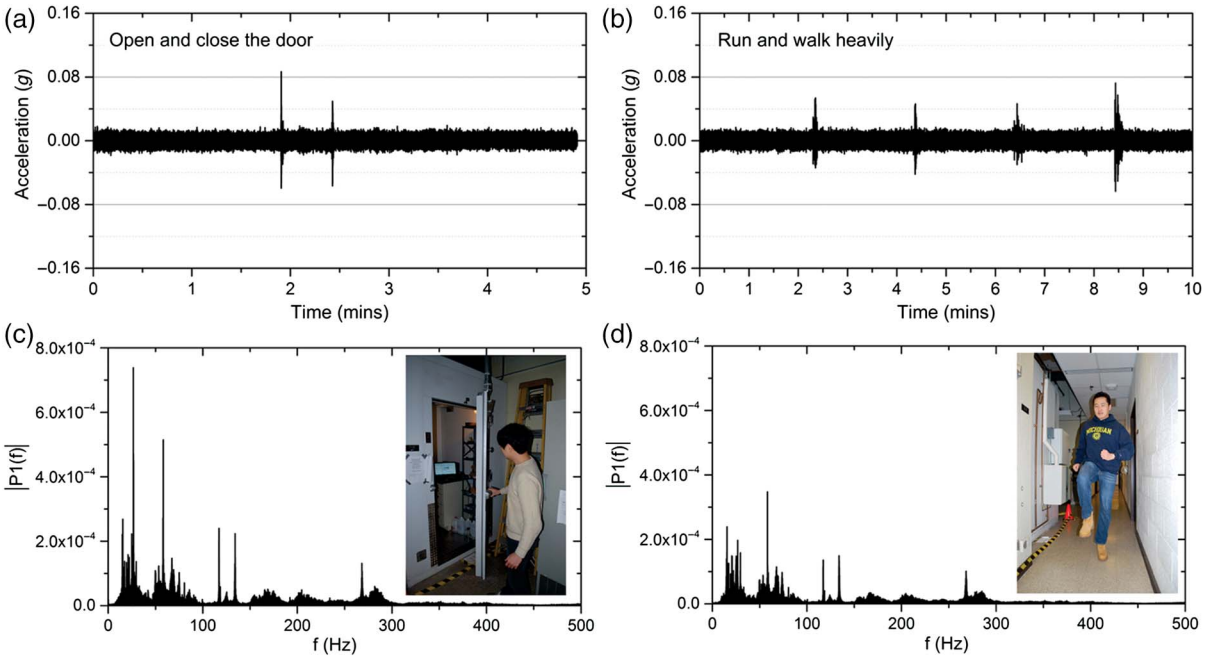

sudden increase in convergence on day 7.1 was a result of external excitation, and these vibrations were likely caused by a person opening and closing the door of the chamber.

Summary and Conclusions

The behavior of silica sand under moderate sustained loads is largely affected by the processes taking place at intergranular contacts. Therefore, grain-scale testing is crucial to finding the causes of aging and time-dependent response of sand to loads. Of particular interest is the time-dependent behavior of contacts subjected to constant (sustained) loads. However, such testing is challenging because of the size of the specimens and the distribution of textural features on grain surfaces being unique to every grain. Measuring the displacement of hundreds of nanometers adds to the challenge. These measurements are also sensitive to changes in temperature and humidity, and are affected by even small vibration excitations.

In order to gain insight into time-dependent microscopic behavior of contacts, an apparatus was constructed that is capable of measuring grain-scale displacements associated with sustained contact loads. Testing a contact between two grains was found inherently inaccurate because of creep in adhesive used for mounting the grains and the use of multiple stages (with their inherent tolerances in the rails) needed to form an intergranular contact. Consequently, an apparatus was constructed for testing grain contacts with steel surfaces; such contacts are equally indicative of sand grain contact behavior. The design allowed for elimination of adhesive from the specimen preparation and also elimination of multiple stages. The displacement measured by the device is the result of the simultaneous response of two contacts of the grain with two polished steel surfaces, on opposite sides of the grain. The displacement of one loading plate relative to the one on the opposite side of the grain is measured, and it is referred to as a *convergence*. While this is not the same as a contact between two grains, the measurements are indicative of the very same time-dependent characteristics.

The purpose of the apparatus constructed is to measure the time-dependent characteristics of contacts. Test results on silica sand grains indicate the contacts to be active for more than 3 weeks after application of the load to the grain. There is a need for testing of grains with diverse origin and texture and under various loads in an effort to gain solid evidence that would support or disprove the static fatigue hypothesis of silica sand aging. The results from testing of individual contacts are also expected to deliver information that will be used in developing contact models applicable in simulations of large assemblies of grains.

ACKNOWLEDGMENTS

The work presented in this paper was supported by the National Science Foundation through grant No. 1537222 from the Division of Civil, Mechanical and Manufacturing Innovation. This support is gratefully acknowledged.

References

Afifi, S. S. and Woods, R. D., 1971, "Long-Term Pressure Effects on Shear Modulus of Soils," *ASCE J. Soil Mech. Found. Div.*, Vol. 97, No. 10, pp. 1445–1460.

Anderson, D. G. and Stokoe, K. H., 1978, "Shear Modulus: A Time-Dependent Soil Property," *Dynamic Geotechnical Testing, ASTM STP654*, M. L. Silver and D. Tiedemann, Eds., ASTM International, West Conshohocken, PA, pp. 66–90.

Bowman, E. T. and Soga, K., 2005, "Mechanisms of Setup of Displacement Piles in Sand: Laboratory Creep Tests," *Can. Geotech. J.*, Vol. 42, No. 5, pp. 1391–1407, https://doi.org/10.1139/t05-063

Brzesowsky, R. H., Spiers, C. J., Peach, C. J., and Hangx, S. J. T., 2011, "Failure Behavior of Single Sand Grains: Theory Versus Experiment," *J. Geophys. Res.*, Vol. 116, No. B6, pp. 1–13, https://doi.org/10.1029/2010JB008120

Cavarretta, I., Coop, M. R., and O'Sullivan, C., 2010, "The Influence of Particle Characteristics on the Behaviour of Coarse Grained Soils," *Géotechnique*, Vol. 60, No. 6, pp. 413–423, https://doi.org/10.1680/geot.2010.60.6.413

Cavarretta, I., Rocchi, I., and Coop, M. R., 2011, "A New Interparticle Friction Apparatus for Granular Materials," *Can. Geotech. J.*, Vol. 48, pp. 1829–1840, https://doi.org/10.1139/t11-077

Charles, R. J., 1958, "Static Fatigue of Glass. I," *J. Appl. Phys.*, Vol. 29, No. 11, pp. 1549–1553, https://doi.org/10.1063/1.1722991

Chow, F. C., Jardine, R. J., Brucy, F., and Nauroy, J. F., 1997, "Time-Related Increases in the Shaft Capacities of Driven Piles in Sand," *Géotechnique*, Vol. 47, No. 2, pp. 353–361, https://doi.org/10.1680/geot.1997.47.2.353

Ciprian, R. and Lehman, B., 2009, "Modeling Effects of Relative Humidity, Moisture, and Extreme Environmental Conditions on Power Electronic Performance," presented at the *IEEE Energy Conversion Congress and Exposition*, San Jose, CA, Institute of Electrical and Electronics Engineers, Piscataway, NJ, https://doi.org/10.1109/ECCE.2009.5316423

Cole, D. M., Mathisen, L. U., Hopkins, M. A., and Knapp, B. R., 2010, "Normal and Sliding Contact Experiments on Gneiss," *Granular Matter*, Vol. 12, No. 1, pp. 69–86, https://doi.org/10.1007/s10035-010-0165-z

Cole, D. M. and Peters, J. F., 2008, "Grain-Scale Mechanics of Geologic Materials and Lunar Simulants under Normal Loading," *Granular Matter*, Vol. 10, pp. 171–185, https://doi.org/10.1007/s10035-007-0066-y

Cuellar, E., Roberts, D., and Middleman, L., 1987, "Static Fatigue Lifetime of Optical Fibers in Bending," *Fiber Integr. Opt.*, Vol. 6, No. 3, pp. 203–213, https://doi.org/10.1080/01468038708223680

Daramola, O., 1980, "Effect of Consolidation Age on Stiffness of Sand," *Géotechnique*, Vol. 30, No. 2, pp. 213–216, https://doi.org/10.1680/geot.1980.30.2.213

Jardine, R. J., Standing, J. R., and Chow, F. C., 2006, "Some Observations of the Effects of Time on the Capacity of Piles Driven in Sand," *Géotechnique*, Vol. 56, No. 4, pp. 227–244, https://doi.org/10.1680/geot.2006.56.4.227

Krauskopf, K. B., 1959, "The Geochemistry of Silica in Sedimentary Environments," *Silica in Sediments* (SP7), H. A. Ireland, Ed., The Society of Economic Paleontologists and Mineralogists, Tulsa, OK, pp. 4–19.

Krinsley, D. H. and Doornkamp, J. C., 1973, *Atlas of Quartz Sand Surface Textures*, Cambridge University Press, Cambridge, UK, pp. 30–91.

Krumbein, W. C., 1941, "Measurement and Geological Significance of Shape and Roundness of Sedimentary Particles," *J. Sediment. Petrol.*, Vol. 11, No. 2, pp. 64–72.

Lade, P. V. and Karimpour, H., 2010, "Static Fatigue Controls Particle Crushing and Time Effects in Granular Materials," *Soils Found.*, Vol. 50, No. 5, pp. 573–583, https://doi.org/10.3208/sandf.50.573

Mesri, G., Feng, T. W., and Benak, J. M., 1990, "Postdensification Penetration Resistance of Clean Sand," *J. Geotech. Eng.*, Vol. 116, No. 7, pp. 1095–1115, https://doi.org/10.1061/(ASCE)0733-9410(1990)116:7(1095)

Michalowski, R. L. and Nadukuru, S. S., 2012, "Static Fatigue, Time Effects, and Delayed Increase in Penetration Resistance after Dynamic Compaction of Sand," *J. Geotech. Geoenv. Eng.*, Vol. 138, No. 5, pp. 564–574, https://doi.org/10.1061/(ASCE)GT.1943-5606.0000611

Michalowski, R. L. and Nadukuru, S. S., 2014, "Contact Fatigue: A Key Mechanism of Time Effects in Silica Sand," presented at the *International Symposium on Geomechanics from Micro to Macro, IS-Cambridge 2014*, Cambridge, UK, Taylor & Francis, Abingdon, England.

Michalowski, R. L., Wang, Z., and Nadukuru, S. S., 2018, "Maturing of Contacts and Ageing of Silica Sand," *Géotechnique*, Vol. 68, No. 2, pp. 133–145, https://doi.org/10.1680/jgeot.16.P.321

Mitchell, J. K. and Solymar, Z. V., 1984, "Time-Dependent Strength Gain in Freshly Deposited or Densified Sand," *J. Geotech. Eng.*, Vol. 110, No. 11, pp. 1559–1576, https://doi.org/10.1061/(ASCE)0733-9410(1984)110:11(1559)

Schmertmann, J. H., 1991, "The Mechanical Aging of Soils," *J. Geotech. Eng.*, Vol. 117, No. 9, pp. 1288–1330, https://doi.org/10.1061/(ASCE)0733-9410(1991)117:9(1288)

Scholz, C. H., 1972, "Static Fatigue of Quartz," *J. Geophys. Res.*, Vol. 77, No. 11, pp. 2104–2114, https://doi.org/10.1029/JB077i011p02104

Senetakis, K. and Coop, M. R., 2013, "The Development of a New Micro-Mechanical Inter-Particle Loading Apparatus," *Geotech. Test. J.*, Vol. 37, No. 6, pp. 1028–1039, https://doi.org/10.1520/GTJ20120187

Wadell, H., 1932, "Volume, Shape, and Roundness of Rock Particles," *J. Geol.*, Vol. 40, No. 5, pp. 443–451, https://doi.org/10.1086/623964

Wang, W. and Coop, M. R., 2016, "An Investigation of Breakage Behavior of Single Sand Particles Using a High-Speed Microscope Camera," *Géotechnique*, Vol. 66, No. 12, pp. 984–998, https://doi.org/10.1680/jgeot.15.P.247

Wang, Z. and Michalowski, R. L., 2015, "Contact Fatigue in Silica Sand—Observations and Modeling," *J. Geomech. Energy Environ.*, Vol. 4, pp. 88–99, https://doi.org/10.1016/j.gete.2015.07.003

Wichtmann, T. and Triantafyllidis, Th., 2004, "Influence of a Cyclic and Dynamic Loading History on Dynamic Properties of Dry Sand, Part I: Cyclic and Dynamic Torsional Prestraining," *Soil Dyn. Earthquake Eng.*, Vol. 24, No. 2, pp. 127–147, https://doi.org/10.1016/j.soildyn.2003.10.004

Wiederhorn, S. M. and Bolz, L. H., 1970, "Stress Corrosion and Static Fatigue of Glass," *J. Am. Ceram. Soc.*, Vol. 53, No. 10, pp. 543–548, https://doi.org/10.1111/j.1151-2916.1970.tb15962.x

Wiederhorn, S. M., Yi, F., LaVan, D., Richter, L. J., Fett, T., and Hoffmann, M. J., 2015, "Volume Expansion Caused by Water Penetration into Silica Glass," *J. Am. Ceram. Soc.*, Vol. 98, No. 1, pp. 78–87, https://doi.org/10.1111/jace.13264

York, D. L., Brusey, W. G., Clémente, F. M., and Law, S. K., 1994, "Setup and Relaxation in Glacial Sand," *J. Geotech. Eng.*, Vol. 120, No. 9, pp. 1496–1513, https://doi.org/10.1061/(ASCE)0733-9410(1994)120:9(1498)